Composition dependence of the diffuse scattering in the relaxor ferroelectric compound $(1-x)Pb(Mg_{1/3}Nb_{2/3})O_3-xPbTiO_3$ $(0\leq x\leq 0.40)$

M. Matsuura,[1] K. Hirota,[1] P. M. Gehring,[2] Z.-G. Ye,[3] W. Chen,[3] and G. Shirane[4]
[1]*Institute for Solid State Physics, University of Tokyo, Kashiwa 277-8581, Japan*
[2]*NIST Center for Neutron Research, National Institute of Standards and Technology, Gaithersburg, Maryland 20899-8562, USA*
[3]*Department of Chemistry, Simon Fraser University, Burnaby, British Columbia, Canada V5A 1S6*
[4]*Department of Physics, Brookhaven National Laboratory, Upton, New York 11973-5000, USA*
(Received 17 January 2006; revised manuscript received 18 June 2006; published 26 October 2006)

We have used neutron diffraction to characterize the diffuse scattering in five single crystals of the relaxor ferroelectric $(1-x)Pb(Mg_{1/3}Nb_{2/3})O_3-xPbTiO_3$ (PMN-*x*PT) with $x=0$, 10, 20, 30, and 40%. The addition of ferroelectric $PbTiO_3$ modifies the well-known "butterfly" and "ellipsoidal" diffuse scattering patterns observed in pure PMN ($x=0$), which are believed to be associated with the presence of randomly oriented polar nanoregions. In particular, the anisotropy of the diffuse scattering diminishes as the PT content increases. The spatial correlation length ξ along the $[1\bar{1}0]$ direction derived from the width of the diffuse scattering at room temperature increases from 12.6 Å for PMN to 350 Å for PMN-20%PT. In addition, the diffuse scattering intensity at $q=0$ grows and reaches a maximum value around the morphotropic phase boundary (MPB), which suggests that it is proportional to the dielectric susceptibility. Beyond $x=30\%$, a concentration very close to the MPB, no diffuse scattering is observed below T_C, and well-defined critical behavior appears near T_C. By contrast, the diffuse scattering for $x\leq 20\%$ persists down to low temperatures, where the system retains an average cubic structure ($T_C=0$). Finally, the anisotropic soft transverse optic (TO) modes observed in PMN are found to be isotropic for PMN-30%PT, which strongly suggests a connection between the anisotropic diffuse scattering and the TO modes.

DOI: 10.1103/PhysRevB.74.144107 PACS number(s): 77.80.−e, 61.12.−q, 77.84.Dy

I. INTRODUCTION

Relaxor ferroelectrics with the general chemical formula $Pb(BB')O_3$ are receiving a great deal of scientific attention because single crystals of their solid solution with the ferroelectric $PbTiO_3$ exhibit extremely high piezoelectric responses.[1–3] Relaxors are distinguished by a broad and highly frequency-dependent peak in the dielectric susceptibility as a function of temperature that does not correspond to a macroscopic change in crystal structure. A key concept that is believed to be central to the mechanism responsible for the high piezoelectricity is that of polar nanoregions (PNRs), which are nanometer-scale regions having local, randomly oriented, ferroelectric polarizations. The existence of such regions was proposed by Burns and Dacol to explain the observed deviation of the optical refraction index of $Pb(Mg_{1/3}Nb_{2/3})O_3$ (PMN), and other disordered materials, from a linear temperature dependence that occurs below a temperature T_d, which is several hundred degrees higher than the Curie temperature T_C.[4,5] Neutron scattering measurements by Naberezhnov *et al.* on PMN revealed the onset of strong diffuse scattering at or very near T_d,[6] also known as the Burns temperature, thereby establishing a plausible connection between the PNRs and the diffuse scattering.

The temperature dependence of the diffuse scattering in the relaxor ferroelectric compound $(1-x)Pb(Mg_{1/3}Nb_{2/3})O_3-xPbTiO_3$ (PMN-*x*PT) has been measured for small values of the PT concentration x and found to vary drastically depending on the measurement technique. Figure 1 shows the thermal variations of the diffuse intensity near the (300) Bragg reflection for PMN-10%PT measured by (a) neutron[7] and (b) x-ray diffraction.[8] Intensity contours of the diffuse scattering for the PMN-*x*PT system resemble a butterfly or ellipsoidal pattern depending on the location in reciprocal space, as shown in the inset of Fig. 1(a). The diffuse intensity detected by neutron diffraction grows monotonically on cooling, while that by x-ray diffraction exhibits critical behavior at T_C.

Unlike a normal ferroelectric system, pure PMN retains an average cubic structure upon zero-field cooling down to 5 K.[9,10] When a dc electric field is applied along the cubic $\langle 111\rangle$ direction in PMN, a field-induced cubic to rhombohedral phase transition occurs upon cooling. The induced ferroelectric phase and the related macroscopic polarization remain stable after the field is removed at low temperatures. Upon subsequent zero-field heating, a spontaneous rhombohedral to cubic phase transition takes place at $T_C=213$ K. This temperature is independent of the initial including field strength.[2] Figure 2 shows the phase diagram of the PMN-*x*PT system. The crosses in Fig. 2 indicate the temperature at which the real part of the dielectric constant is maximum (T_{max}) at a frequency of 1 kHz.[11] The crystal structure of PMN-*x*PT was studied by x-ray diffraction for $x=5$, 10, and 15 % polycrystals by Ye *et al.*,[12] and an $x=10\%$ single crystal by Dkhil *et al.*[13] showing a rhombohedral distortion for all concentrations in zero field at low temperatures. However, using high-resolution neutron diffraction on an $x=10\%$ crystal, Gehring *et al.* found no rhombohedral splitting of the (111) Bragg peak down to $T=50$ K ($<T_C=285$ K).[7] A subsequent high-Q-resolution neutron diffraction study for $x=20$ and 27 % by Xu *et al.* found a rhombohedral distortion for $x=27\%$, but not for $x=20\%$.[14] High-energy x-ray and neutron diffraction studies of the related relaxor $Pb(Zn_{1/3}Nb_{2/3})O_3$ (PZN) have shown that the dis-

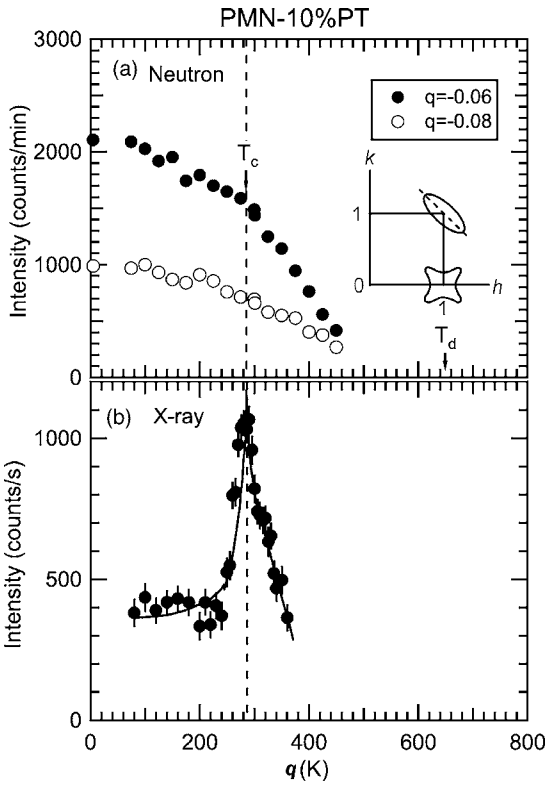

FIG. 1. Temperature dependence of the diffuse scattering in PMN-10%PT measured by (a) neutron scattering (Ref. 7) at $(3qq)$ and (b) x-ray scattering (Ref. 8) near (300). Inset in (a) shows a schematic of the diffuse scattering intensity contours observed in PMN. The dotted line in the inset denotes the trajectory of the q scans shown in Fig. 4.

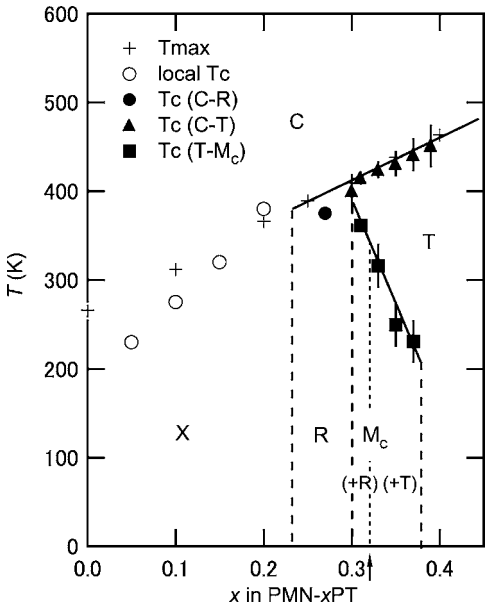

FIG. 2. Zero-field phase diagram of PMN-xPT. Crosses locate the temperature at which the real part of the dielectric constant, measured at a frequency of 1 kHz by Noblanc *et al.*, is maximum (Ref. 11). Open circles denote the value of the local T_C at which either a zero-field- or field-induced cubic (C) to rhombohedral (R) transition was observed for PMN, and a structural phase transition was observed by x-ray diffraction (Refs. 12 and 13), or by dielectric measurements ($0.05 \leq x \leq 0.15$, Ref. 11), but not by neutron diffraction (Refs. 7 and 14). A bulk C to R phase transition, however, was observed for $x=0.27$. For $0.31 \leq x \leq 0.37$, the PMN-xPT system exhibits a cubic to tetragonal (T) phase transition on cooling, and then a monoclinic major phase (Mc) at low temperatures, which coexists with the R phase on the lower-PT side (PMN-31%PT) and the T phase on the higher-PT side ($33 \leq x \leq 37\%$).[17]

crepancy between x-ray and neutron scattering results comes from a difference between the structure of the skin, or outer region, of the crystal (which is rhombohedral) and that of the interior, or bulk of the crystal (which has a cubic unit cell, i.e., the so-called phase X).[15,16] Therefore, the values of the field-induced T_C for PMN and the T_C determined by x-ray diffraction for $x \leq 20\%$ will henceforth be denoted as "local T_C" (T_C^{loc}) as it appears that the ferroelectric distortion is limited to short range in the bulk of PMN-xPT crystals for $x \leq 20\%$. Around the morphotropic phase boundary (MPB), which had been considered to be a sharp compositional boundary between the rhombohedral and tetragonal phases, a monoclinic phase of M_C type was found to coexist with a rhombohedral or tetragonal phase at lower temperatures.[17] The values of T_C determined by x-ray structural studies for $x \geq 30\%$ match well with T_{max}. For $x \geq 40\%$, only a tetragonal phase appears at low temperatures as in ferroelectric $PbTiO_3$. The frequency dependence of the peak in the dielectric susceptibility, which is characteristic of relaxors, disappears for $x \geq 40\%$, indicating that normal ferroelectric behavior exists in the tetragonal phase of PMN-xPT.

The microscopic mechanism responsible for the diffuse scattering, which is important for the relaxor behavior, is not fully understood. The purpose of this study is to elucidate the evolution of the diffuse scattering from the relaxor to ferroelectric state. We have performed neutron scattering experiments on PMN-xPT single crystals of $x=0$, 10, 20, 30, and 40 %. We have concentrated on the diffuse scattering around the (110) and (100) Bragg reflections, and measured the intensity contours, q profiles, and temperature dependences. By studying the evolution of the diffuse scattering with temperature, we present evidence that the PNRs develop into macroscopic polar domains below T_C for $x \geq 30\%$. For $T > T_C$, the diffuse scattering intensity at $q=0$ as a function of the PT content achieves a maximum value near the MPB, which suggests that it corresponds to the dielectric susceptibility. We also discuss a possible correlation between the anisotropic diffuse scattering and the low-frequency TO modes.

II. EXPERIMENTAL DETAILS

The samples used in this study are all high-quality PMN-xPT single crystals. The $x=0$ and 10% samples were grown from a high-temperature solution at Simon Fraser University, while the $x=20$, 30, and 40 % crystals were kindly provided by Rutgers University (20%), and Virginia Tech (30 and 40 %). The samples are rectangular in shape with a volume of 0.50, 0.30, 0.125, 0.09, and 0.08 cm^3 for $x=0$, 10, 20, 30, and 40 %, respectively. The energy-integrated intensity of

the TO phonon measured at the wave vector $\vec{Q}=(2.15,1.85,0)$ is proportional to the sample volume, and all data have been normalized accordingly. All of the neutron scattering experiments reported here were performed on the ISSP triple-axis spectrometers HER and PONTA, both of which are located at the JRR-3 reactor of the Japan Atomic Energy Agency. The incident neutron energies E_i were selected using the (002) Bragg reflection of a highly oriented pyrolytic graphite (HOPG) monochromator. The data obtained on the HER spectrometer were collected using "cold" neutrons of incident energy $E_i=5$ meV ($\lambda=4.04$ Å), a cooled Be filter placed in front of the sample to suppress neutrons with higher-order wavelengths, and horizontal beam collimations of guide-open-*S*-80′-80′(*S*=sample). The data taken on the PONTA spectrometer were collected using "thermal" neutrons of energy $E_i=14.7$ meV ($\lambda=2.36$ Å), two HOPG filters placed before and after the sample, and two different horizontal beam collimations of 15′-80′-*S*-20′-80′ and 40′-80′-*S*-40′-80′. Each crystal was mounted onto a boron nitride post with tantalum wire, or a copper plate with copper wire, and attached to the cold head of a closed-cycle helium refrigerator. The samples were then mounted with the cubic [001] axis (*c* axis) vertical to provide access to Bragg reflections of the form (*hk*0) during the experiments. In order to compare diffuse scattering measurements from all samples directly, all the reciprocal space contours and profiles shown in this report are plotted on the same intensity scale after normalizing the data by crystal volume and counting time. Reciprocal lattice units (rlu) are used, where 1 rlu$=2\pi/a$, and $a=4.045$ Å (PMN), 4.037 Å (10%), 4.028 Å (20%), 4.027 Å (30%), 4.023 Å (40%) are the room-temperature cubic lattice parameters.

III. RESULTS

A. Diffuse scattering

Figure 3 shows the contours of constant diffuse scattering intensity measured near the reciprocal lattice positions $\vec{Q}=(110)$ and (100) at $T=300$ K for both the PMN and PMN-10%PT samples. These data were taken on the HER spectrometer, which, because of the use of cold neutrons, provides better instrumental energy and Q resolutions than does the PONTA spectrometer. We note that the diffuse scattering patterns shown for our PMN sample are consistent with those reported in previous studies of PMN.[18–20] Near (110) a strong ridge of diffuse scattering extends along the direction transverse to $\vec{Q}$ ($[1\bar{1}0]$) while a much weaker ridge extends along the longitudinal direction ([110]). Near (100) the diffuse scattering is elongated equally along the [110] and $[1\bar{1}0]$ directions, resulting in the well-known butterfly pattern. With the substitution of 10%PT we find that the shape of the diffuse scattering changes slightly. In particular, near both (100) and (110), the extent of the diffuse scattering along the $[1\bar{1}0]$ and [110] directions is lessened relative to that for PMN such that the intensity contours become less anisotropic in appearance. The effect of the PT content on the diffuse scattering in the PMN-*x*PT system thus differs from that in the PZN-*x*PT system in as much as almost the same diffuse scattering intensity contours were observed for both PZN and PZN-8%PT, and PZN-8%PT is much closer to the morphotropic phase boundary than is PMN-10%PT.[21]

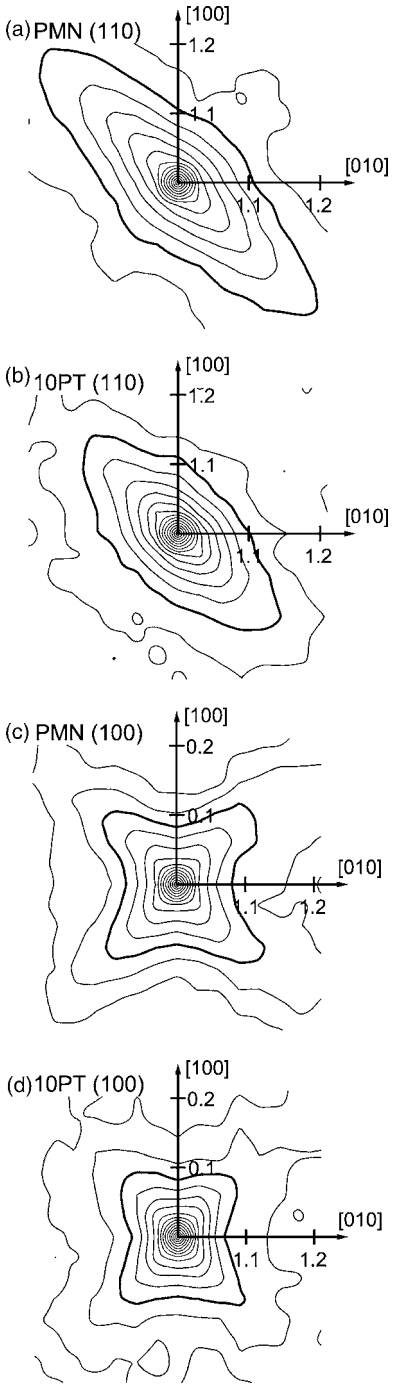

FIG. 3. Constant intensity contours of the diffuse scattering near (110) and (100) for PMN and PMN-10%PT measured at room temperature. Each contour corresponds to a logarithmic change in intensity of 0.25 (base 10). Thick lines represent the contour intensity of $10^{2.3}\sim 200$(arb. units). Counts are plotted on the same intensity scale after normalizing by crystal volume and counting time.

Several diffuse scattering intensity profiles, measured at $T=300$ K near (110) along the $[1\bar{1}0]$ direction, are presented

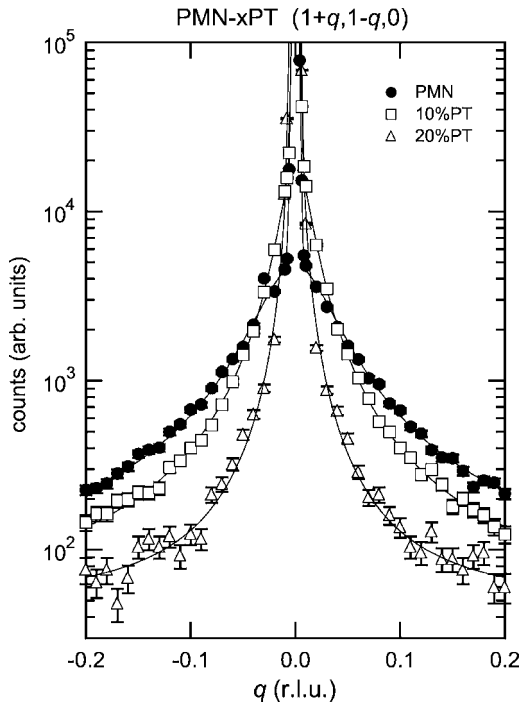

FIG. 4. Diffuse scattering measured near (110) along the $[1\bar{1}0]$ direction at room temperature for PMN, PMN-10%PT, and PMN-20%PT. Intensities are plotted on a logarithmic scale. The q-scan trajectory is shown schematically in the inset of Fig. 1(a). Solid lines are fits to the data as described in the text.

in Fig. 4 as a function of the reduced wave vector q [measured relative to $\vec{Q}=(110)$] for different PT concentrations. Each profile contains a narrow, resolution-limited peak from the (110) Bragg reflection and a broad peak corresponding to the diffuse scattering. In order to estimate the width of the diffuse scattering peak, which is of interest because it is inversely proportional to the spatial correlation length of the polar nanoregions, these data were fit to the sum of a Lorentzian and a Gaussian function of q, representing the diffuse and Bragg scattering contributions, respectively, convolved with the Gaussian instrumental resolution function. The Lorentzian function is parametrized by

$$f(q) = \frac{I_0}{\pi}\frac{\kappa}{q^2+\kappa^2},$$

where I_0 is the integrated intensity, and κ is the half width at half maximum (HWHM). The values of the fitted parameters are listed in Table I. The correlation length ($\xi=1/\kappa$) for pure PMN is found to be 12.6 Å, which is consistent with the value reported in a previous study.[20] This agreement provides a useful check of both the data and the fitting procedure. We note that the fitting errors for the case of PMN-20%PT are large because the width of the diffuse scattering peak has narrowed to such an extent that it is comparable to that of the (110) Bragg peak, thereby making it difficult to distinguish between them. From this analysis we conclude that, as the PT concentration increases, the HWHM decreases while the integrated intensity increases. This suggests that the change in the diffuse scattering contours with increasing PT content shown in Fig. 3 is in fact not due simply to an overall reduction in the strength of the diffuse scattering, but rather to a decrease in the peak width, which reflects a growth in the correlation length of the PNR. In addition, an enhancement of the intensity at $q=0$, $I_0/(\kappa\pi)$, was observed with increasing PT concentration. The PT dependence of $I_0/(\kappa\pi)$ is similar to that of the dielectric constant, which grows with increasing PT content up to the MPB.

It is possible that differences in the shapes of the diffuse scattering contours between different compositions at 300 K are the result of differences in the temperature dependence of the diffuse scattering, given that T_C^{loc} increases linearly with the PT content x as shown in Fig. 2. To test this possibility we measured the temperature dependence of the diffuse scattering profiles near (110) along the $[1\bar{1}0]$ direction for both the PMN-10%PT and PMN-20%PT samples. Figure 5 shows the temperature dependence of the fitting parameters, which were determined by the same method as those shown in Table I. The data points for PMN were measured by Xu *et al.* near (100) along the $[1\bar{1}0]$ direction.[20] The integrated intensity I_0 has been normalized to 1 at $T=300$ K. We find that the thermal variations of I_0 for the PMN-10%PT and PMN-20%PT crystals are quite similar to that for PMN reported by Xu *et al.*[20] On cooling, the diffuse scattering starts growing around 500 K and continues to increase even below T_C^{loc}. The spatial correlation length ξ of the diffuse scattering at temperatures above 500 K has a constant value ~10 Å for PMN-10%PT and PMN-20%PT, which is almost the same as that for PMN. The value of ξ increases rapidly on cooling at the respective T_C^{loc}: 213 K (PMN), 275 K (PMN-10%PT), and 380 K (PMN-20%PT), and then saturates at lower temperatures. As shown in Table I, the correlation length for PMN-10%PT at $T=300$ K ($>T_C^{loc}=275$ K) is three times larger than that for PMN. In addition, the limiting value of ξ for PMN-10%PT at low temperature (100 K) is ~200 Å, which is also three times as large as that for PMN ($\xi=60$ Å).[20] This indicates that the width of the diffuse scattering in PMN-10%PT along the ridge direction is reduced

TABLE I. Fitting parameters characterizing the diffuse scattering near (110) along the $[1\bar{1}0]$ direction at $T=300$ K.

PMN-xPT	I_0	κ (rlu)	ξ (Å)	$I_0/(\kappa\pi)$ (arb. units)
0	539±4	0.0362±0.0004	12.6±0.1	4730±150
10%	837±4	0.0135±0.0001	33.7±0.3	19800±600
20%	1970±420	0.0013±0.0003	350±80	$4.8\pm3.6\times10^5$

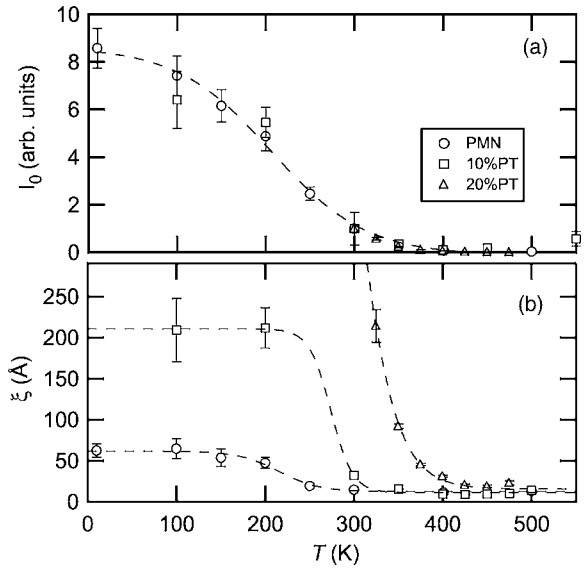

FIG. 5. Temperature dependence of the normalized integrated intensity I_0 and correlation length ξ extracted from fits to q scans of the diffuse scattering near (110) along the $[1\bar{1}0]$ direction for the PMN-10%PT and PMN-20%PT samples. Data for PMN were taken from published results by Xu *et al.* (Ref. 14) measured near (100) along the $[1\bar{1}0]$ direction. The parameter I_0 has been normalized to 1 at $T=300$ K. Dashed lines in (a) and (b) are guides to the eye.

by a factor of 3 compared to that in PMN over the entire temperature range. As shown in Table I, the integrated intensity parameter I_0 at 300 K increases with the PT content. Together with the longer correlation lengths, our data analysis shows that substitution with ferroelectric $PbTiO_3$ gives stronger and sharper diffuse scattering while preserving the overall temperature dependence of I_0.

If the temperature dependence of the diffuse scattering does not change with the PT content, then the contour shape of the diffuse scattering should depend only on the anisotropy of ξ. At 300 K, the diffuse scattering in PMN-10%PT is more isotropic than that in PMN. Since the anisotropy of ξ may change with temperature, we compared the contour shapes of the diffuse scattering in PMN and PMN-10%PT at a temperature where the ξ measured along the ridge direction has almost the same value. Figure 6 shows diffuse scattering contours for PMN-10%PT near (110) at $T=400$ K at which

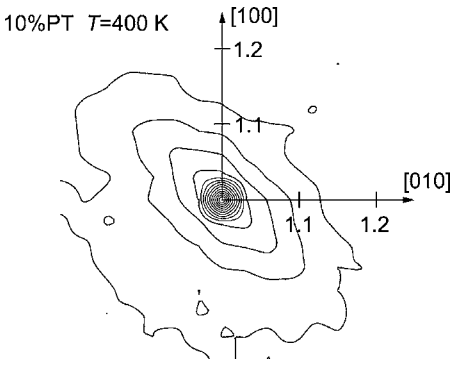

FIG. 6. Intensity contours of the diffuse scattering near (110) for PMN-10%PT measured at 400 K.

ξ along the ridge direction has almost the same value (9.4 Å) as that for PMN at $T=300$ K. The shape of the diffuse scattering for PMN-10%PT at $T=400$ K is not similar to that for PMN at $T=300$ K, but rather to that for PMN-10%PT itself at $T=300$ K; the ellipsoidal diffuse scattering becomes more isotropic (than that of PMN) over the entire temperature range.

We performed a series of q scans around the (110) Bragg reflection for each of the PMN-20%PT, PMN-30%PT, and PMN-40%PT samples to characterize the diffuse scattering at PT concentrations near and beyond the morphotropic phase boundary. Figure 7 shows diffuse scattering contours both below T_C (300 K) and just above T_C (T_C+10 K) for each crystal. With increasing the PT content the shape of the contours evolves from ellipsoidal to circular just above T_C while the contours become more densely packed around the zone center; even so, there is still evidence of weak diffuse scattering intensity for PMN-40%PT. Below T_C, a drastic decrease in the diffuse intensity is seen between PMN-20%PT and PMN-30%PT. For PMN-20%PT, the diffuse scattering persists below T_C^{loc} with a very narrow peak width along the transverse direction, corresponding to a correlation length $\xi=350\pm80$ Å that is close to the resolution limit. For PMN-30%PT and PMN-40%PT below T_C, however, there is almost no diffuse scattering around (110), as is clear from the way that the thick contours, which correspond to an intensity of 200 counts, shrink toward the (110) Bragg peak below T_C. The shoulder visible at (1.03,0.97,0) for PMN-40%PT is associated with the tetragonal distortion (with $a=3.995$ Å and $c=4.05$ Å) below T_C. There is also a rhombohedral distortion for PMN-30%PT at $T=300$ K($<T_C$), but it is not visible given the coarse beam collimations used here. Since the ferroelectric distortion is not present in the bulk for $x=20\%$ (phase X), but is present for 27%,[14] the disappearance of the diffuse scattering for $x\geq30\%$ suggests that diffuse scattering below T_C exists only in the phase X.

B. Critical behavior

If PMN-30%PT and PMN-40%PT are normal ferroelectrics, then the diffuse scattering should exhibit critical behavior near T_C. Figure 8 shows how the diffuse scattering intensity varies with temperature at $(1+q,1-q,0)$ for PMN-20%PT, PMN-30%PT, and PMN-40%PT, for several values of the reduced wave vector q. It is immediately apparent that the behavior of the diffuse scattering for PMN-20%PT is qualitatively different from those of PMN-30%PT and PMN-40%PT. For PMN-20%PT, the intensity at $(1+q,1-q,0)$ for $q\leq0.05$ rlu appears to increase more rapidly below ~450 K. Some evidence of a small kink is seen at T_C^{loc} (370 K); below this temperature we note that the peak intensity of the (200) Bragg peak increases sharply by a factor of 20, which cannot be explained by a thermal (Debye-Waller) factor. Since both longitudinal and transverse q widths of the (200) Bragg peak become larger below T_C^{loc}, an increase of the correlation length can be ruled out. In a nearly perfect crystal, the scattering intensity of a strong Bragg peak becomes smaller than the calculated value. The depletion of the beam intensity due to scattering by various crystallites is called secondary ex-

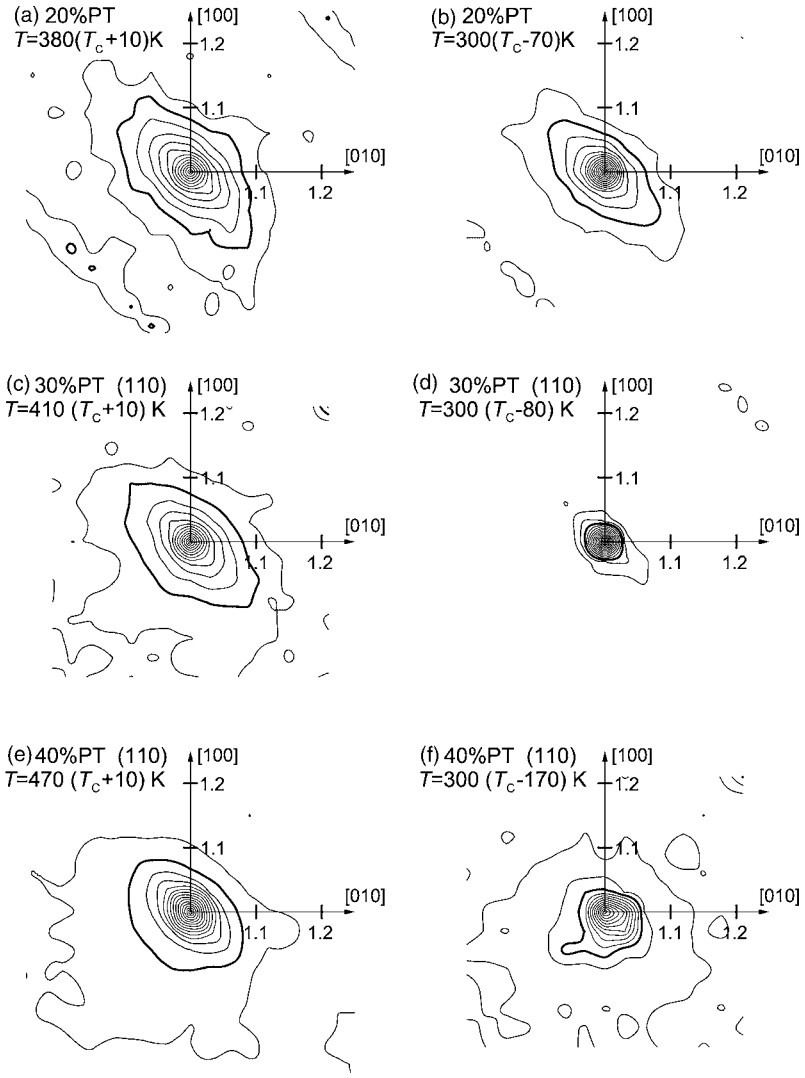

FIG. 7. Intensity contours of the diffuse scattering near (110) for PMN-20%PT, PMN-30%PT, and PMN-40%PT measured below (300 K) and above T_C. Thick lines represent contours of intensity of $10^{2.3} \sim 200$, the same as shown in Fig. 3.

tinction; primary extinction describes the related process in a perfect single crystal due to coherent reductions in beam intensity from scattering by individual lattice planes. We speculate that the crystallites tilt away from each other below T_C^{loc}, which reduces the secondary extinction effect. On further cooling below T_C^{loc}, the intensity measured at $q=0.02$ rlu continues to grow while that measured at $q=0.03$ and 0.05 does not. This results in a narrower diffuse peak around (110) at lower temperatures. Thus, the diffuse scattering for PMN-20%PT is anomalous in that it persists below T_C. By contrast, critical behavior is observed for PMN-30%PT and PMN-40%PT near T_C. The intensities for PMN-30%PT rise and fall on cooling and exhibit a plateau over a 30 K temperature range. The intensities at $(1+q,1-q,0)$ with $q=0.03$, 0.04, and 0.05 rlu increase on cooling from high temperature, but then display kinks as indicated by arrows. A value of $T_C=402$ K was determined from an extrapolation of the temperatures of the kinks to that at $q=0$. Below this temperature, the intensities remain constant for about 30 K and then decrease gradually on cooling. A second $T_C=377$ K was determined from an identical extrapolation of the kinks observed at lower temperatures. These T_C's are consistent with the structural phase transition temperatures obtained from x-ray studies by Noheda *et al.*; successive transitions occur on cooling from cubic to tetragonal, and then from tetragonal to rhombohedral phases around $T=400$ and 350 K, respectively.[17] For PMN-40%PT, the diffuse scattering intensities at $(1+q,1-q,0)$ with $q=0.03$, 0.04, and 0.05 rlu peak at $T=471$, 474, and 477 K, respectively. The extrapolated value of T_C was determined to be 462 K, which is consistent with a phase transition from cubic to tetragonal symmetry around $T=450$ K for $x=39\%$.[17] Thus, the presence of critical behavior is confirmed at the phase transition temperatures corresponding to a ferroelectric distortion in the PMN-xPT samples with $x \geq 30\%$.

C. Lattice dynamics

We have also investigated differences between the lattice dynamics of PMN and PMN-30%PT. Figures 9(a) and 9(b) show constant-Q spectra at $T=550$ K for PMN measured at $Q=(2.15,1.85,0)$ and $(2,-0.21,0)$, respectively. Both of these wave vectors have the same modulus, i.e., both are located a distance of $|q|=0.21$ rlu from the zone center; thus both sets of transverse acoustic (TA) and TO phonon peaks should appear at the same energy if the dispersions are iso-

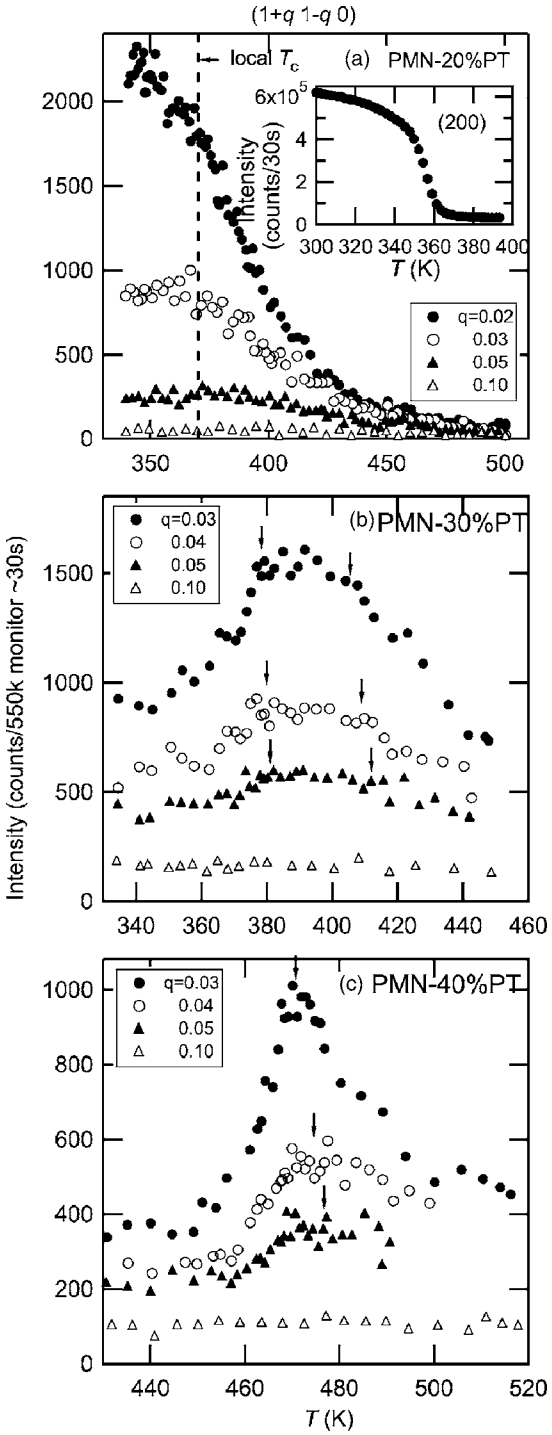

FIG. 8. Temperature dependence of the neutron scattering intensities at $(1+q,1-q,0)$ for PMN-20%PT, PMN-30%PT, and PMN-40%PT. The vertical dashed line in (a) indicates T_C^{loc}, which is determined from the temperature dependence of the (200) Bragg intensity. Arrows indicate those temperatures where the scattering intensities suggest kinks or divergences. The inset in (a) shows the temperature dependence of the scattering intensity at the (200) Bragg peak.

tropic. The solid lines are fits based on a linear dispersion for the TA mode and a flat dispersion for the TO mode; the instrumental resolution is taken into account. A Lorentzian distribution in energy with HWHM Γ was assumed for both phonon cross sections. The TA modes at (2.15,1.85,0) and (2,−0.21,0) appear at the same frequency $\hbar\omega = 3.8 \pm 0.1$ meV, while the TO mode at (2.15,1.85,0) appears at a lower frequency (9.0±0.2 meV) than that at (2, −0.21,0) (10.8±0.1 meV). Assuming the dispersion of the TO mode varies as $\omega^2 = \Omega_0^2 + Dq^2$, where Ω_0 is the frequency of the zone center TO mode and D is the slope, D was determined to be 420 and 750 meV^2 Å^2 with $\Omega_0^2 = 35$ meV^2 for (2.15,1.85,0) and (2,−0.21,0), respectively. An anisotropic slope of the TO mode in PMN has been observed by Stock *et al.*;[22] however, the anisotropy we observe is much stronger than that of Stock *et al.*, which is presumably due to a difference in measurement temperatures. In addition, the TO mode at (2.15,1.85,0) has a larger energy width ($\Gamma = 2.4 \pm 0.2$ meV) compared to that at (2,−0.21,0) ($\Gamma = 1.4 \pm 0.2$ meV). The TO mode becomes soft and has a larger linewidth along the $[1\bar{1}0]$ direction than does that along the [100] direction. Figures 9(c) and 9(d) show constant-Q spectra at (2.15,1.85,0) and (2,−0.21,0) at $T = 550$ K for PMN-30%PT, respectively. Although the data quality is not good due to the small size of the PMN-30%PT crystal, the TO mode for PMN-30%PT at (2.15,1.85,0) is clearly harder compared to that for PMN and appears at almost the same frequency (10.1±0.3 meV) as that at (2,−0.21,0) (11.1±0.5 meV). This suggests that the addition of PT reduces the anisotropy of the TO modes in PMN.

IV. DISCUSSION

A. Spatial correlations of PNRs

We have observed the diffuse scattering just above T_C or T_C^{loc} for PMN-xPT up to $x=40\%$. The diffuse scattering has an ellipsoidal shape and a butterfly one around the (110) and (100) reciprocal lattice points, respectively. Linear q scans of the diffuse scattering along the ridge directions $[1\bar{1}0]$ for (110), and [1 ±1 0] for (100), were well fitted with a Lorentzian function. Shvartsman *et al.* recently succeeded in directly imaging the PNR in PMN-20%PT by piezoresoponse force microscopy.[23] They found micro-meter-size domains of PNRs containing embedded nanodomains of opposite polarization, indicating a heterogeneous PNRs structure. Since neutron scattering detects the average structure, the inverse HWHM of a Lorentzian peak fit to the diffuse scattering can be regarded as the average correlation length of the PNR.

The spatial correlation length ξ of the PNR changes with temperature; it starts increasing on cooling from temperatures 80–100 K higher than T_C^{loc}, and rapidly rises near T_C^{loc}, then saturates at low temperatures. This temperature dependence was observed for $x \leq 20\%$. The addition of PT enhances the size of the correlation length ξ for $x \leq 20\%$. Compared to the ξ of PMN at room temperature, the ξ values of PMN-10%PT and PMN-20%PT are enhanced by factors of 3 and 30, respectively. In addition, the low-temperature saturation value of ξ for 10%PT is found to be three times larger than that for PMN. This indicates that PT substitution increases the correlation length of the PNR over the entire temperature range. This is consistent with a crystal optical

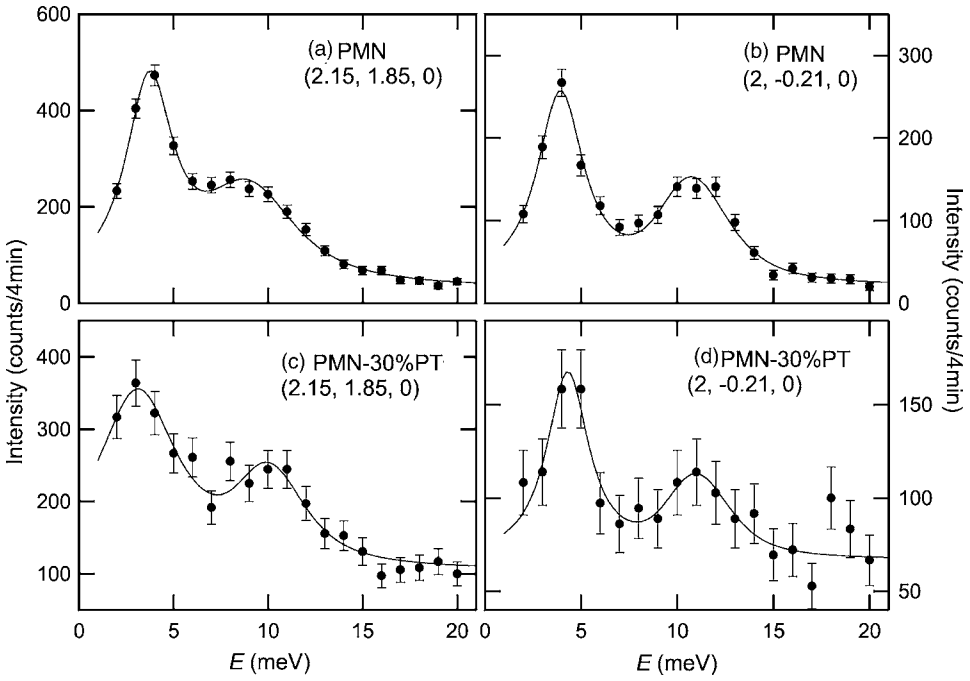

FIG. 9. Constant-Q scans at $T=550$ K showing TA and TO phonon modes at $Q=(2.15,1.85,0)$ and $(2,-0.21,0)$ for PMN and PMN-30%PT.

study,[24] in which the substitution of Ti^{4+} ions for $(Mg_{1/3}Nb_{2/3})^{4+}$ tended to induce larger PNRs, leading to macroscopic polar domains.

B. Diffuse scattering intensity at $q=0$

We have found that the diffuse scattering intensity at $q=0$, $I_0/(\kappa\pi)$, at $T=300$ K grows with the PT content up to $x=20\%$, as shown in Table I. Although we cannot compare the diffuse scattering intensity at $q=0$ at $T=300$ K for PMN-30%PT and PMN-40%PT because the diffuse scattering disappears below $T_C(>300$ K), Fig. 8 shows that the diffuse scattering near T_C in PMN-40%PT is weaker than that in PMN-30%PT. Together with the enhancement in $I_0/(\kappa\pi)$ for $x\leq 20\%$, our data indicate that the diffuse scattering intensity at $q=0$ exhibits a maximum near the MPB as a function of the PT content. The observed PT dependence of the diffuse scattering intensity at $q=0$ is similar to that of the dielectric constant, which suggests a close correlation between the diffuse scattering and the dielectric susceptibility.

C. Appearance of critical behavior

We have observed that the diffuse scattering disappears below T_C for PMN-30%PT and PMN-40%PT. Furthermore, critical behavior is observed near the structural phase transition temperatures. Since the anisotropic diffuse scattering is associated with short-range polar order, the disappearance of the diffuse scattering indicates the establishment of long-range ferroelectric order associated with a long-range structural distortion below T_C for $x\geq 30\%$. On the other hand, the diffuse scattering for $x\leq 20\%$ grows on cooling even below T_C^{loc}, that is, in the phase X. As shown in the inset of Fig. 8(a), the peak intensity of the nuclear Bragg reflection is enhanced below T_C^{loc}, which can be explained by a release of secondary extinction due to the formation of domains. This indicates that some short-range ferroelectric distortion exists in the phase X, even though there is no clear bulk rhombohedral splitting. Together with the PT and temperature dependences of the size of the PNRs, the following scenario can be naturally deduced. For $x\leq 20\%$, randomly oriented PNRs appear at T_d and begin to develop correlations on cooling. The correlation of the PNRs increases under the influence of the effective field produced by the polarizations in neighboring domains. However, below T_C^{loc}, the growth of the PNR is prevented for $x\leq 20\%$PT, presumably by quenched compositional disorder, resulting in an average cubic phase with a local ferroelectric distortion.

D. Q pattern of diffuse scattering

In addition to enhancing the correlation length of the PNR, PT substitution affects the shape of the diffuse scattering. As shown by the thick reference lines in Fig. 3, the extent of the diffuse scattering contours in PMN-10%PT around (100) narrows along the [110] directions compared to those in pure PMN, i.e., the "wings" of the butterfly pattern become smaller. This demonstrates that the addition of PT to PMN reduces the anisotropy of the diffuse scattering in reciprocal space. At the same time the extent of the diffuse scattering contours along the transverse direction (along [010]) remains constant. That the scattering along this direction does not diminish suggests that a gradual evolution is taking place toward the situation for a classical displacive ferroelectric wherein the softening of the TO mode gives rise to critical scattering intensity at zero energy near the Γ point that extends along the transverse Q direction. With further PT substitution above 30%, the transverse component around (110) becomes weak, and the contours around (110) change from an ellipse to a circle. The ratio of the long axis to the short axis of the ellipse represented by the thick line decreases from 2.8 (PMN), to 2.3 (10%PT), 1.8 (20%PT), 1.7

(30%PT), and 1.5 (40%PT). Recent high-energy x-ray diffraction by Stock *et al.* revealed no transverse diffuse scattering in PMN-60%PT.[25] Since the dielectric constant for $x \geq 40\%$PT shows a sharp peak at the first-order ferroelectric phase transition temperature T_C which no longer depends on frequency, this suggests a close correlation between the transverse diffuse scattering and the relaxor behavior.

E. Anisotropic TO modes

We have measured the anisotropic soft TO mode at $T = 550$ K in PMN. This mode exhibits a lower frequency and a larger linewidth along the $[1\bar{1}0]$ direction near (220) than that measured along the [010] direction near (200). The diffuse scattering in the PMN-*x*PT system has been shown to extend along the six ⟨110⟩ directions perpendicular to the wave vector Q.[18–20] Thus, it is reasonable to speculate that the observed anisotropic diffuse scattering in PMN originates from the condensation of the soft TO mode, as this mode is strongly damped and thus should produce some scattering at zero energy. However, a recent neutron spin-echo study on PMN by Vakhrushev *et al.* has shown that the diffuse scattering in PMN is purely elastic with an accuracy of 1 μ eV.[26] We therefore speculate that the soft TO phonon may be trapped by local crystal distortions produced by the PNRs, which in turn produces a central peak as is seen in $SrTiO_3$.[27] Such crystal distortions could be associated with the uniform displacement of the PNRs, a concept introduced by Hirota *et al.* to reconcile the measured diffuse scattering and phonon intensities in PMN.[28] Xu *et al.* have recently performed a three-dimensional mapping of the diffuse scattering in a single crystal of the relaxor PZN using x-ray scattering techniques, which exhibits the same diffuse contour shapes as found in PMN, and were able to simulate the diffuse scattering intensity by assuming six ⟨110⟩-type polarization directions.[20]Such polarizations may trap TO modes especially along the six ⟨110⟩ directions. In PMN-30%PT, both the TO mode dispersions and the diffuse scattering become isotropic, supporting our speculation.

Recently, Stock *et al.* performed a systematic inelastic neutron scattering study on PMN and discovered a strong temperature dependence to both the energy and linewidth of the TA mode near (110), where the diffuse scattering is strong. This suggests a coupling between the diffuse scattering and the acoustic mode.[25] Further work is required to clarify the nature of the coupling between the central component, TO modes, TA modes, and the reciprocal space distribution of the diffuse scattering.

V. CONCLUSIONS

We have characterized the temperature and composition dependences of the diffuse scattering in the PMN-*x*PT solid solution system. The spatial correlation length associated with the PNR is enhanced by PT substitution, resulting in the eventual establishment of long-range ferroelectric order and the appearance of a macroscopic critical behavior for samples with $x \geq 30\%$. The anisotropic diffuse scattering, which extends along the six ⟨110⟩ directions, becomes increasingly isotropic as the PT content increases. The anisotropic soft TO modes along the ⟨110⟩ direction observed in PMN are found to be isotropic for PMN-30%PT, which indicates a coupling between the anisotropic diffuse scattering and the TO modes.

ACKNOWLEDGMENTS

We would like to thank G. Xu and C. Stock for stimulating discussions. This study was partially supported by the U.S.-Japan Cooperative Program on Neutron Scattering. We are very grateful to D. Viehland and V. Kiryukhin for letting us carry out neutron scattering experiments on their crystals (PMN-20%PT, PMN-30%PT, and PMN-40%PT). Work done by Z.-G. Ye and W. Chen at Simon Fraser University was supported by the U.S. Office of Naval Research Grant No. 00014-06-1-0166.

[1] S.-E. Park and T. R. Shrout, J. Appl. Phys. **82**, 1804 (1997).
[2] Z.-G. Ye, Key Eng. Mater. **155-156**, 81 (1998).
[3] A. A. Bokov and Z.-G. Ye, J. Mater. Sci. **41**, 31 (2006).
[4] G. Burns and F. H. Dacol, Solid State Commun. **48**, 853 (1983).
[5] PMN exhibits no structural transition in zero field. Thus T_C is not defined. However, PMN has been reported to transform to a rhombohedral phase near 210 K when cooled in a field of at least 1.8 kV/cm. When we refer to T_C for PMN in this paper, it should be understood that we are referring to the field-cooled transition temperature of 210 K.
[6] A. Naberezhnov, S. Vakhrushev, B. Dorner, D. Strauch, and H. Moudden, Eur. Phys. J. B **11**, 13 (1999).
[7] P. M. Gehring, W. Chen, Z.-G. Ye, and G. Shirane, J. Phys.: Condens. Matter **16**, 7113 (2004).
[8] B. Dkhil, J. M. Kiat, G. Calvarin, G. Baldinozzi, S. B. Vakhrushev, and E. Suard, Phys. Rev. B **65**, 024104 (2002).
[9] P. Bonneau, P. Garnier, E. Husson, and A. Morell, Mater. Res. Bull. **24**, 201 (1989).
[10] N. de Mathan, E. Husson, G. Calvarin, J. R. Gavarri, A. W. Hewat, and A. Morell, J. Phys.: Condens. Matter **3**, 8159 (1991).
[11] O. Noblanc, P. Gaucher, and G. Calvarin, J. Appl. Phys. **79**, 4291 (1996).
[12] Z.-G. Ye, Y. Bing, J. Gao, A. A. Bokov, P. Stephens, B. Noheda, and G. Shirane, Phys. Rev. B **67**, 104104 (2003).
[13] B. Dkhil, J. M. Kiat, G. Calvarin, G. Baldinozzi, S. B. Vakhrushev, and E. Suard, Phys. Rev. B **65**, 024104 (2002).
[14] G. Xu, D. Viehland, J. F. Li, P. M. Gehring, and G. Shirane, Phys. Rev. B **68**, 212410 (2003).
[15] K. Ohwada, K. Hirota, P. W. Rehrig, Y. Fujii, and G. Shirane, Phys. Rev. B **67**, 094111 (2003).
[16] G. Xu, P. M. Gehring, C. Stock, and K. Conlon, Phase Transitions **79**, 135 (2006).
[17] B. Noheda, D. E. Cox, G. Shirane, J. Gao, and Z.-G. Ye, Phys.

Rev. B **66**, 054104 (2002).
[18] S. B. Vakhrushev, A. A. Naberezhnov, N. M. Okuneva, and B. N. Savenko, Phys. Solid State **37**, 1993 (1995).
[19] H. Hiraka, S.-H. Lee, P. M. Gehring, G. Xu, and G. Shirane, Phys. Rev. B **70**, 184105 (2004).
[20] G. Xu, G. Shirane, J. R. D. Copley, and P. M. Gehring, Phys. Rev. B **69**, 064112 (2004).
[21] D. La-Orauttapong, J. Toulouse, Z.-G. Ye, W. Chen, R. Erwin, and J. L. Robertson, Phys. Rev. B **67**, 134110 (2003).
[22] C. Stock *et al.*, Phys. Rev. B **73**, 064107 (2006).
[23] V. V. Shvartsman and A. L. Kholkin, Phys. Rev. B **69**, 014102 (2004).
[24] Z.-G. Ye and M. Dong, J. Appl. Phys. **87**, 2312 (2000).
[25] C. Stock, H. Luo, D. Viehland, J. F. Li, I. Swaison, R. J. Birgeneau, and G. Shirane, J. Phys. Soc. Jpn. **74**, 3002 (2005).
[26] S. Vakhrushev, A. Ivanov, and J. Kulda, Phys. Chem. Chem. Phys. **7**, 2340 (2005).
[27] S. M. Shapiro, J. D. Axe, and G. Shirane, Phys. Rev. B **6**, 4332 (1972).
[28] K. Hirota, Z.-G. Ye, S. Wakimoto, P. M. Gehring, and G. Shirane, Phys. Rev. B **65**, 104105 (2002).